

PAPER

A 2-D Image Stabilization Algorithm for UWB Pulse Radars with Fractional Boundary Scattering Transform

Takuya SAKAMOTO^{†a)}, *Member*

SUMMARY The UWB (ultra-wideband) pulse radar is a promising candidate as an environment measurement method for rescue robots. Radar imaging to locate a nearby target is known as an ill-posed inverse problem, on which various studies have been done. However, conventional algorithms require long computational time, which makes it difficult to apply them to real-time operations of robots. We have proposed a fast radar imaging algorithm, the SEABED algorithm, for UWB pulse radars. This algorithm is based on a reversible transform, BST (Boundary Scattering Transform), between the target shape and the observed data. This transform enables us to estimate target shapes quickly and accurately in a noiseless environment. However, in a noisy environment the image estimated by the SEABED algorithm is degraded because BST utilizes differential operations. We have also proposed an image stabilization method, which utilizes the upper bound of the smoothness of received data. This method can be applied only to convex objects, not to concave ones. In this paper, we propose a fractional BST, which is obtained by expanding the conventional BST, and an image stabilization method by using the fractional BST. We show that the estimated image can be stabilized regardless of the shape of target.

key words: ultra-wideband (UWB) pulse radar, shape estimation, SEABED algorithm, boundary scattering transform (BST), stabilization, fractional BST (FBST)

1. Introduction

The ultra-wideband (UWB) pulse radar is a strong candidate as a method for environment measurement for rescue robots, which are thought to be realizable in the near future. Radar imaging for targets close to an antenna is known as an ill-posed inverse problem, on which various studies have been done. Synthetic aperture processing is one such study, in which resolution is limited to half the wavelength [1]–[3]. A migration algorithm is often used for seismic investigations, and was also used for the radar imaging with the finite-difference time-domain (FDTD) method [4]. A domain integral equation is another approach that expresses the target with many permittivity parameters assigned to all grids of the space, which enables us to apply this method to general problems [5]–[7]. The discrete model fitting method expresses the target boundary by using a set of point targets, which suitably reduce the degree of freedom, and images are obtained by optimization algorithms [8]. These algorithms require long calculation times because they are based on iterative computations, which makes it difficult to apply them

to the real-time operations required for robotics.

We have proposed a fast shape estimation algorithm for UWB pulse radars in order to solve the above problem [9]–[13]. This algorithm is called the SEABED algorithm, and it utilizes the boundary scattering transform that is a reversible transform between the target shape and the received data. The SEABED algorithm does not require an iterative computation, and it can directly estimate target shapes from the data by the inverse transform. Because the boundary scattering transform utilizes the derivative of a quasi wavefront, which is an estimated curve from the received signals, it degrades the estimated image in a noisy environment. To overcome this problem, we have derived an inequality of the upper bound that guarantees the smoothness of the quasi wavefronts for convex targets. This inequality was effectively utilized to develop a smoothing algorithm that enables us to stably estimate a target shape [14]. Although this method works well for convex targets, the estimation error becomes rather large for concave targets. In this paper, we propose an image stabilization algorithm that can be used for any target shape. First, we expand the boundary scattering transform and obtain a fractional boundary scattering transform. The fractional boundary scattering transform enables us to deal with the intermediate space (fractional transform space) between a real space and a data space. In the fractional transform space, the quasi wavefront is smooth for various target shapes. Therefore, stable imaging is achieved by utilizing the fractional boundary scattering transform. Furthermore, we also derive the optimum parameter of the fractional transform, which enables us to adaptively utilize the fractional transform depending on the target shape, and enhance estimation accuracy.

2. System Model

We assume a mono-static radar system. An omni-directional antenna is scanned along a straight line. UWB pulses are transmitted at a fixed interval and received by the antenna. The received data is A/D converted and stored in a memory. We estimate target shapes using the obtained data. Figure 1 shows the system model.

We deal with a 2-dimensional problem. Targets and the antenna are located on a plane. We define a real space where targets and the antenna are located. We express the real space with the parameters (x, y) . Both x and y are normalized by λ , which is the center wavelength of the transmitted pulse in air. We assume $y > 0$ for simplicity. The

Manuscript received January 23, 2006.

Manuscript revised August 9, 2006.

[†]The author is with the Department of Communications and Computer Engineering, Graduate School of Informatics, Kyoto University, Kyoto-shi, 606-8501 Japan.

a) E-mail: t-sakamo@i.kyoto-u.ac.jp

DOI: 10.1093/ietcom/e90-b.1.131

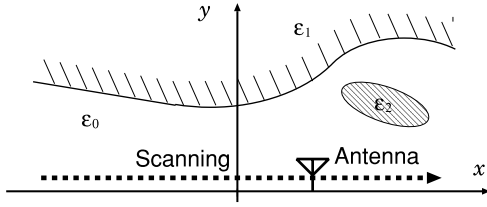


Fig. 1 The coordinates and an example of a target complex permittivity.

antenna is scanned along the x -axis in r -space. We define $s'(X, Y)$ as the received electric field at the antenna location $(x, y) = (X, 0)$, where we define Y with time t and the speed of the radiowave c as $Y = ct/(2\lambda)$. We apply a matched filter of the transmitted waveform for $s'(X, Y)$. We define $s(X, Y)$ as the output of the filter. We define a data space expressed by (X, Y) . The transform from the data space to the real space corresponds to the imaging we deal with in this paper.

3. SEABED Algorithm

3.1 Boundary Scattering Transform and Its Inverse Transform

We developed a fast radar imaging algorithm based on BST (Boundary Scattering Transform) [9]–[13]. We call the algorithm SEABED (Shape Estimation Algorithm based on BST and Extraction of Directly scattered waves). The algorithm utilizes the existence of a reversible transform BST between target shapes and pulse delays. We have clarified that the SEABED has the advantage of direct estimation of target boundaries using inverse transform, a mathematically complete solution for the inverse problem. We assume that each target has a uniform complex permittivity, and is surrounded by a clear boundary. We also assume that the propagation speed is known. Here, we assume the medium of the direct path is a vacuum for simplicity.

The upper figure in Fig. 2 shows an example of a target shape. A strong scatter is received from the point P in the figure. The distance Y between the point P and the antenna $(X, 0)$ is easily obtained by a UWB radar. The relationship between X and Y is shown in the lower figure in Fig. 2. We call this curve a quasi wavefront. The BST is expressed as

$$X = x + y \frac{dy}{dx}, \quad (1)$$

$$Y = y \sqrt{1 + \left(\frac{dy}{dx}\right)^2}, \quad (2)$$

where (X, Y) is a point on a quasi wavefront, and (x, y) is a point on the target boundary [9]. We have clarified that the inverse transform of the BST is given by

$$x = X - YdY/dX, \quad (3)$$

$$y = Y \sqrt{1 - (dY/dX)^2}, \quad (4)$$

where we assume $|dY/dX| \leq 1$. This condition is required

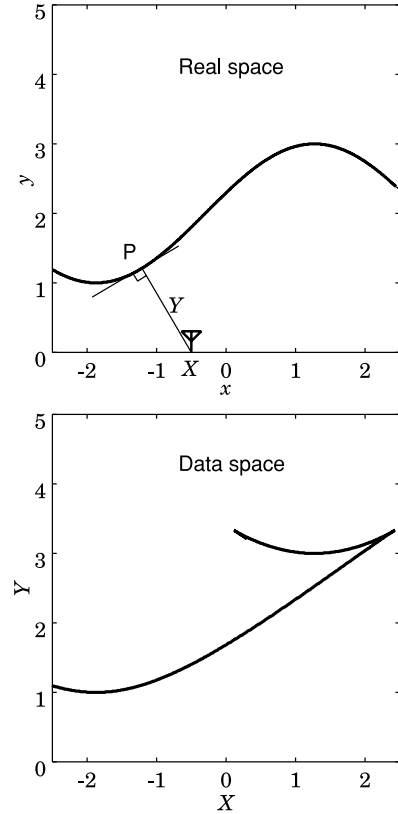


Fig. 2 An example of a target shape and a quasi wavefront.

because y should be a real number. This condition can be utilized as a clue to estimate the quasi wavefronts from the received signals. We call the transform in Eqs. (3) and (4) Inverse Boundary Scattering Transform (IBST).

First, quasi wavefronts are extracted from the received signals $s(X, Y)$ in the SEABED algorithm. Quasi wavefronts are extracted to satisfy the conditions $ds(X, Y)/dY = 0$ and $|dY/dX| \leq 1$. Next, we select quasi wavefronts with a large evaluation value that is calculated by summing the signal power along the estimated quasi wavefront. Finally, we apply the IBST to the quasi wavefronts, and obtain the final image.

3.2 Smoothing of Quasi Wavefronts

The algorithm mentioned in the previous subsection works well in a noiseless environment. However, real signals contain noise, which leads to random components in the quasi wavefronts estimated from the signals. The differential operation in the IBST can amplify this random component, which then degrades the estimated image. To solve this problems, we proposed an image stabilization algorithm that applies smoothing to quasi wavefronts by utilizing the upper bound of the 2nd derivative of the quasi wavefront for convex targets [14]. A smoothing with a long correlation length can be applied if the absolute value of the 2nd derivative is small. The 2nd derivative of the quasi wavefront is expressed as

$$\frac{d^2 Y}{dX^2} = \frac{\frac{d^2 y}{dx^2}}{\left\{1 + \left(\frac{dy}{dx}\right)^2\right\}^{3/2} \left\{1 + \left(\frac{dy}{dx}\right)^2 + y \frac{d^2 y}{dx^2}\right\}}. \quad (5)$$

The numerator in this equation is the 2nd derivative of the target shape $\frac{d^2 y}{dx^2}$, which depends on the target shape. The term in the denominator $\left\{1 + \left(\frac{dy}{dx}\right)^2\right\}^{3/2}$ is always larger than 1, which diminishes the absolute value of the 2nd derivative. On the other hand, as for the term in the denominator $1 + \left(\frac{dy}{dx}\right)^2 + y \frac{d^2 y}{dx^2}$,

1. for a convex target

$1 + \left(\frac{dy}{dx}\right)^2 + y \frac{d^2 y}{dx^2} > 1$ is satisfied because $\frac{d^2 y}{dx^2} > 0$ holds. It can be easily smoothed.

2. for a point target or an edge point

The cancellation of $\frac{d^2 y}{dx^2}$ in both the numerator and the denominator makes the 2nd derivative small. It can be easily smoothed.

3. for a concave target

$y \frac{d^2 y}{dx^2} < 0$ is added to $1 + \left(\frac{dy}{dx}\right)^2 > 1$ if $\frac{d^2 y}{dx^2} < 0$. It can lead to $1 + \left(\frac{dy}{dx}\right)^2 + y \frac{d^2 y}{dx^2} < 1$. This is difficult to smooth.

Smoothing quasi wavefronts is effective in cases 1 and 2 above to obtain a stable image. However, the smoothing of quasi wavefronts cannot work for case 3 above, and it degrades the estimated image. In this paper, we propose a stabilization algorithm that can be applied to any targets regardless of their shape.

4. Fractional Boundary Scattering Transform

4.1 Fractional Boundary Scattering Transform and Its Inverse Transform

In this section, we introduce a fractional boundary scattering transform obtained by expanding conventional boundary scattering transform. Next, we propose a smoothing algorithm with the fractional boundary scattering transform. We define the fractional boundary scattering transform, FBST (α) as

$$x_\alpha^B = x + \alpha y \frac{dy}{dx}, \quad (6)$$

$$y_\alpha^B = y \sqrt{1 + \alpha \left(\frac{dy}{dx}\right)^2}. \quad (7)$$

Equations (6) and (7) contain a parameter α ($0 \leq \alpha \leq 1$), which is not included in the conventional boundary scattering transform. We call (x_α^B, y_α^B) a fractional transform quasi wavefront. We call the space expressed with (x_α^B, y_α^B) a fractional transform space. The fractional transform quasi wavefront is equivalent to the conventional quasi wavefront for $\alpha = 1$. On the other hand, the fractional transform quasi wavefront is equivalent to the target shape for $\alpha = 0$.

Similarly, the fractional inverse boundary scattering

transform, FIBST (α) is defined as

$$x_\alpha^I = X - \alpha Y \frac{dY}{dX}, \quad (8)$$

$$y_\alpha^I = Y \sqrt{1 - \alpha \left(\frac{dY}{dX}\right)^2}. \quad (9)$$

We call the left-hand side of Eqs. (8) and (9) a fractional inverse transform quasi wavefront. The left-hand side of Eq. (9) becomes a real number if $0 \leq \alpha \leq 1$ because any quasi wavefront satisfies $|dY/dX| < 1$ [9]. These transforms, FBST and FIBST, can deal with the intermediate space between a real space and a data space.

4.2 The Uniqueness of the Fractional Transform Space

We define fractional transform quasi wavefront vectors $\mathbf{f}_B(\alpha) = [x_\alpha^B, y_\alpha^B]^T$ and $\mathbf{f}_I(\alpha) = [x_\alpha^I, y_\alpha^I]^T$. A target shape can be expressed with these vectors in two ways as

$$\begin{bmatrix} x \\ y \end{bmatrix} = \mathbf{f}_B(0) = \mathbf{f}_I(1). \quad (10)$$

Similarly, a quasi wavefront can be expressed as

$$\begin{bmatrix} X \\ Y \end{bmatrix} = \mathbf{f}_B(1) = \mathbf{f}_I(0). \quad (11)$$

We investigate the relationship between the FBST and FIBST for general α . Solving Eq. (2) for dy/dx , and substituting Eq. (4) to it, we obtain

$$\frac{dy}{dx} = \frac{dY/dX}{\sqrt{1 - (dY/dX)^2}}. \quad (12)$$

Substituting Eqs. (1), (2), and (12) to Eqs. (7) and (6), we obtain

$$x_\alpha^B = X - (1 - \alpha) Y \frac{dY}{dX}, \quad (13)$$

$$y_\alpha^B = Y \sqrt{1 - (1 - \alpha) \left(\frac{dY}{dX}\right)^2}. \quad (14)$$

These equations are equivalent to the FIBST in Eqs. (8) and (9), if we replace α by $1 - \alpha$. This means that the FBST (α) of a target shape is equivalent to the FIBST ($1 - \alpha$) of the quasi wavefront. We can define a fractional transform space and a fractional inverse transform space without any contradiction because the uniqueness is confirmed above. This can be also written as $\mathbf{f}_B(\alpha) = \mathbf{f}_I(1 - \alpha)$. We do not need to utilize a fractional inverse transform quasi wavefront, and we deal with only a fractional transform quasi wavefront in the following sections. Additionally, we do not have to distinguish the left-hand side terms of FBST and FIBST, and we simply express $[x_\alpha, y_\alpha]^T = [x_\alpha^B, y_\alpha^B]^T$.

4.3 The Inverse Transform of the Fractional Boundary Scattering Transform

We showed that the transform from the real space and the

data space to the fractional transform space can be defined without a contradiction. In this section, we show the transform from the fractional transform space to a real space. This transform is equivalent to the inverse transform of the FBST. Equation (7) can be also written as

$$x_\alpha = x + (\sqrt{\alpha}y) \frac{d(\sqrt{\alpha}y)}{dx}, \quad (15)$$

$$\sqrt{\alpha}y_\alpha = \sqrt{\alpha}y \sqrt{1 + \left(\frac{d(\sqrt{\alpha}y)}{dx}\right)^2}. \quad (16)$$

This equation can be obtained by applying the transformation of variables as $y \rightarrow \sqrt{\alpha}y$ and $y_\alpha \rightarrow \sqrt{\alpha}y_\alpha$ to the conventional BST. Its inverse transform can immediately be derived because it can be obtained only by the same transformation of variables of the IBST. The inverse transform of Eq. (16) is expressed as

$$x = x_\alpha - \alpha y_\alpha \frac{dy_\alpha}{dx_\alpha}, \quad (17)$$

$$y = y_\alpha \sqrt{1 - \alpha \left(\frac{dy_\alpha}{dx_\alpha}\right)^2}. \quad (18)$$

We easily see that Eq. (18) is nothing but the fractional inverse boundary scattering transform FIBST (α). Similarly, we can confirm that the inverse transform of the FIBST is the FBST. By utilizing these characteristics, it is possible to obtain the target shape estimation by applying a FIBST after applying another FIBST.

We have defined and used FBST (α) and FIBST (α) for $0 \leq \alpha \leq 1$, which effectively avoided a confusing explanation by distinguishing the forward and inverse transforms. However, it is obvious that $\text{FBST}(\alpha) = \text{FIBST}(-\alpha)$ holds for $-1 \leq \alpha \leq 1$. For example, $\text{FBST}(-1)$ is equal to the IBST, and $\text{FIBST}(-1)$ is equal to the BST. We can simultaneously deal with the forward transform and inverse transform by assuming $-1 \leq \alpha \leq 1$. We generalize the FBST, with Eqs. (6) and (7) for $-1 \leq \alpha \leq 1$. We do not deal with the FIBST in the following description. We can describe the procedure that deals with a boundary scattering transform by dividing it into two pieces as

$$\text{FBST}(1) = \text{FBST}(\alpha) + \text{FBST}(1 - \alpha) \quad (19)$$

by expressing multiple transforms as their summation. In this expression, the FBST has linearity in regard to its parameter α . Similarly, the existence of the inverse transform of the BST in the conventional SEABED algorithm can be expressed as

$$\text{FBST}(0) = \text{FBST}(1) + \text{FBST}(-1), \quad (20)$$

where $\text{FBST}(0)$ is an identity transform. By utilizing the linearity of the BST, the existence of the inverse transform can be interpreted as $1 + (-1) = 0$. Figure 3 shows the relationship among the FBST and the conventional BST.

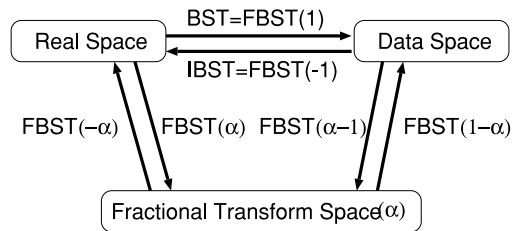


Fig. 3 The relationships of the spaces.

4.4 Characteristics of a FBST

As mentioned above, the smoothing processing scarcely degrades the obtained image for a convex target because the 2nd derivative of the quasi wavefront of a convex surface is smooth. On the other hand, the smoothing processing degrades images of concave surfaces. The fractional transform is the key idea to resolve this problem. The 2nd derivative of a fractional transform quasi wavefront is expressed as

$$\frac{d^2 y_\alpha}{dx_\alpha^2} = \frac{\frac{d^2 y}{dx^2}}{\left\{1 + \alpha \left(\frac{dy}{dx}\right)^2\right\}^{3/2} \left\{1 + \alpha \left(\frac{dy}{dx}\right)^2 + \alpha y \frac{d^2 y}{dx^2}\right\}}. \quad (21)$$

For $\alpha = 0$, this equation is equivalent to the numerator, which is the 2nd derivative of the target shape. For $\alpha = 1$, this equation is equivalent to the 2nd derivative of the conventional quasi wavefront as in Eq. (5). The roughness of the quasi wavefront of a concave surface is caused by the denominator of Eq. (21), $1 + \alpha \left(\frac{dy}{dx}\right)^2 + \alpha y \frac{d^2 y}{dx^2}$. Note that $\frac{d^2 y}{dx^2} < 0$ holds for concave surfaces that cancel the positive term $1 + \alpha \left(\frac{dy}{dx}\right)^2$, which easily gets close to the singular. The condition of $\frac{d^2 y}{dx^2}$ that guarantees the regularity of Eq. (21) is

$$\frac{d^2 y}{dx^2} > -\frac{1}{y} \left\{ \frac{1}{\alpha} + \left(\frac{dy}{dx}\right)^2 \right\}. \quad (22)$$

This condition shows that $\alpha < 1$ is better than $\alpha = 1$ to regularize Eq. (21). However, $\left|\frac{d^2 y_\alpha}{dx_\alpha^2}\right|$ becomes large when the numerator $\frac{d^2 y}{dx^2}$ is large if $\alpha \approx 0$. We propose a smoothing algorithm in the fractional transform space of $0 < \alpha < 1$ as a compromise of these factors. Figure 4 shows the relationship between the 2nd derivative of a target shape $d^2 y/dx^2$ and the absolute value of the 2nd derivative of the fractional transform quasi wavefront $|d^2 y_\alpha/dx_\alpha^2|$, where we assume $y = 1$ and $dy/dx = 0$ for simplicity. The target shape has the largest 2nd derivative for $d^2 y/dx^2 > 0$. The quasi wavefront has the largest 2nd derivative for $d^2 y/dx^2 < 0$. On the other hand, the fractional transform quasi wavefront ($\alpha = 0.5$) does not have the largest 2nd derivative for any $d^2 y/dx^2$. It is possible to apply a smoothing algorithm with a long correlation length by utilizing a fractional transform quasi wavefront regardless of the target shape.

Please note that it is not guaranteed that the fractional transform space ($\alpha = 0.5$) has the smallest maximum value

of $|d^2y_\alpha/dx_\alpha^2|$ for arbitrary shapes. The important thing is that the fractional transform space ($\alpha = 0.5$) has the smallest maximum value of $|d^2y_\alpha/dx_\alpha^2|$ for a certain d^2y/dx^2 if the observer does not have any information about the target shape. Especially if the 2nd order derivative hardly varies within the treated area, it is the best way to set $\alpha=0.5$. From the practical viewpoint, most of artificial objects have edges, where d^2y/dx^2 become considerably large, which is not included in the range $-1 \leq d^2y/dx^2 \leq 1$ in Fig. 4. In such cases, we should apply the smoothing in the data or fractional transform spaces, not in the real space.

Figure 5 shows the proposed smoothing algorithm compared to a conventional smoothing algorithm [14]. In the conventional algorithm, the IBST is applied once after smoothing a quasi wavefront. On the other hand, in the proposed algorithm, a quasi wavefront is transformed by a FBST ($\alpha = -0.5$) to produce a fractional transform quasi wavefront, smoothing is then applied, and finally the FBST ($\alpha = -0.5$) is applied again to obtain a final image. This procedure can be calculated in a short time, and so does

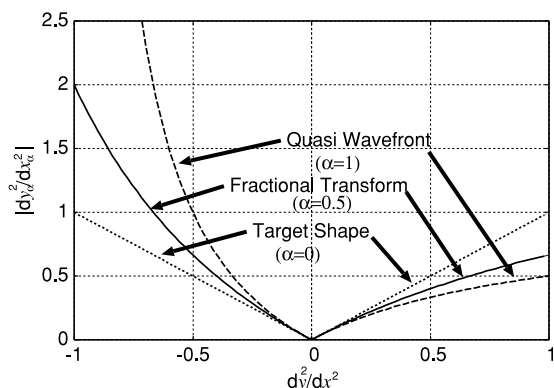


Fig. 4 The relationship between d^2y/dx^2 and d^2y_α/dx_α^2 .

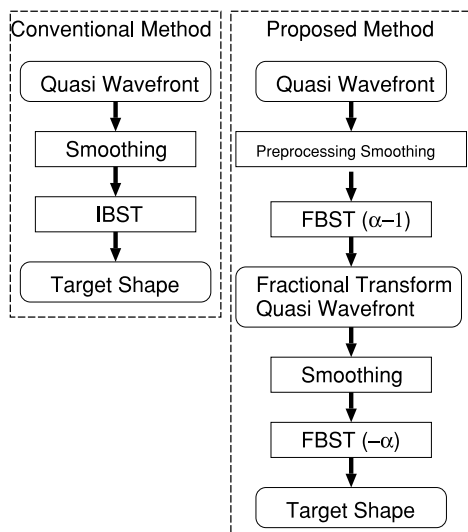


Fig. 5 Procedures of the proposed smoothing method and the conventional one.

not spoil the advantage of quick imaging provided by the SEABED algorithm.

5. Application Examples of the Proposed Algorithm

In this section, we assume the target shape as the solid line in Fig. 6. The target has both convex and concave surfaces. Quasi wavefronts are numerically obtained by applying BST to this target shape. We assume that an antenna is sequentially located at 1000 points along a straight line. We add Gaussian error to the quasi wavefronts, which is an approximation of the additive white Gaussian noise included in received signals. The broken line in Fig. 6 is the quasi wavefront, which is an ideally estimated quasi wavefront from the received data. The quasi wavefront is smoother than the target shape at the convex region. On the other hand, the quasi wavefront is rather sharpened at the concave region. The fractional transform quasi wavefront has a moderate curvature throughout the target surfaces regardless of the shape. In this section we also deal with a stabilization algorithm that applies smoothing to the IBST of the quasi wavefront in order to compare it to others. We apply a preprocessing in which each quasi wavefront is smoothed with a short correlation length, which is set to 2.5×10^{-2} wavelength in this paper. This preprocessing is indispensable for our algorithms because the FIBST (or IBST) contains the derivative operations which are too sensitive to the high-frequency error in the quasi wavefronts. Therefore, we need the smoothing in this preprocessing even for the smoothing in the real space and the fractional transform space as well. We add Gaussian random sequences with a standard deviation of 1.0×10^{-2} wavelength to the ideal quasi wavefront, where the standard deviation corresponds to the strength of the random signals. Especially for the mono-cycle pulse waveform in Fig. 7, the relationship between the signal-to-noise ratio (S/N) and the standard deviation of the Gaussian random error of a quasi wavefront is shown in Fig. 8. Here, we define the S/N as the ratio of peak instantaneous signal power to the averaged noise power after applying the matched filter. In Fig. 8, we see the linear relationship with the inclination of 0.1/20 dB for the S/N larger than 14 dB. The assumed standard devi-

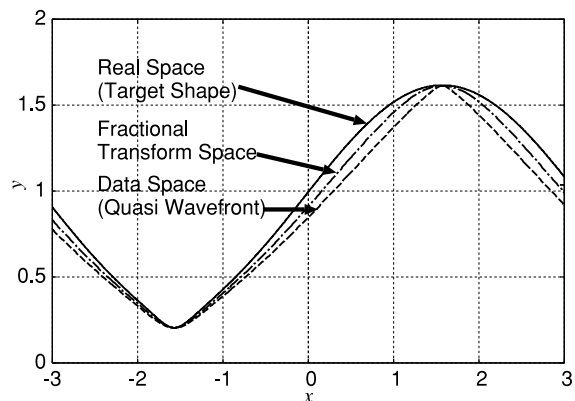


Fig. 6 Example of a FBST.

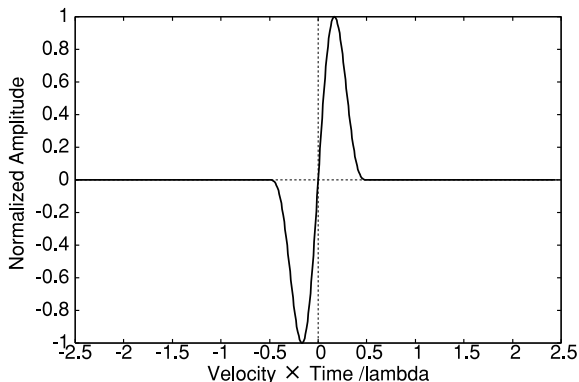


Fig. 7 Assumed mono-cycle pulse waveform.

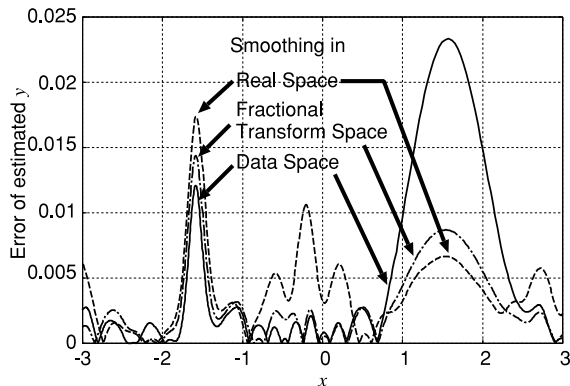


Fig. 10 Error of the estimated shape.

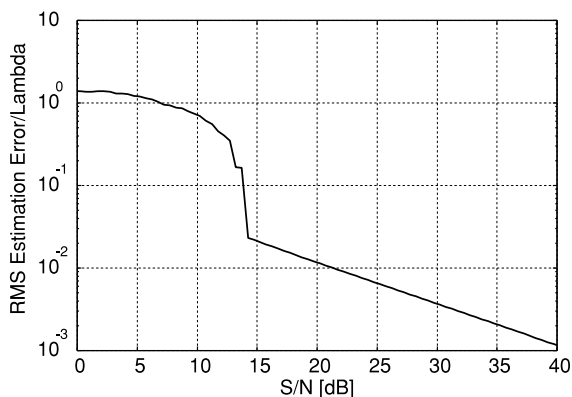


Fig. 8 The relationship between the S/N and the error of quasi wavefront.

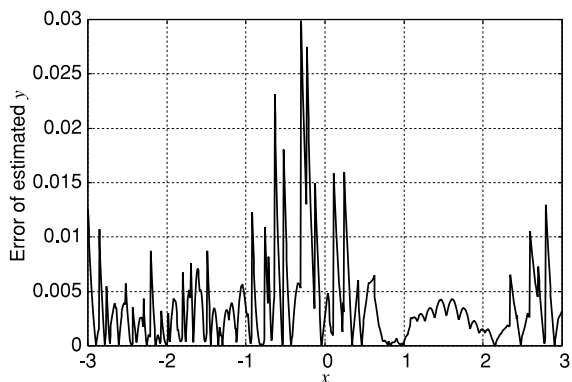


Fig. 9 Error of the estimated shape without smoothing.

ation of 1.0×10^{-2} wavelength corresponds to the S/N of 21.3 dB.

Figure 9 shows the estimation error of the SEABED algorithm without smoothing except for in the above-noted preprocessing, where the absolute value of the error is plotted. We see that error is large at several points, one reaching 0.03 of a wavelength. Figure 10 shows the estimation error of the image by 3 methods where we set $\alpha = 0.5$. The plotted lines in the figure are the absolute values of the errors. Each method applies smoothing with a correlation length of 0.1 of a wavelength. In the convex region, the smoothing in

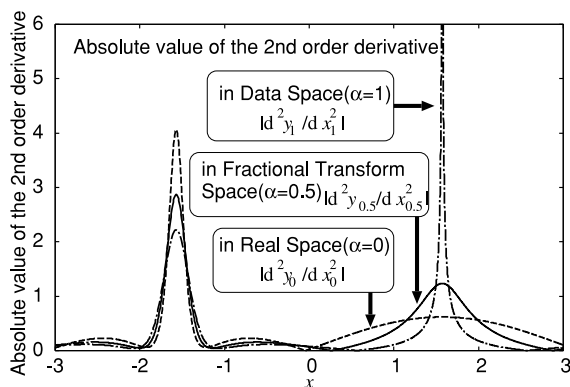


Fig. 11 2nd order derivatives for $\alpha = 0.0, 0.5, 1.0$.

the real space has the largest error. In the concave region, the smoothing in the data space has the largest error. On the other hand, the smoothing in the fractional transform space can accurately estimate the target shape regardless of the target shape. The maximum error with the proposed method is less than 0.015 of a wavelength. This improvement by our proposed method depends on the target shape. The improvement is clearer if the target shape contains the sharper concave than the assumed one. Figure 11 shows the absolute value of the 2nd order derivative in each space, which shows that the 2nd order derivative in the fractional transform space ($\alpha = 0.5$) is unconditionally located between the real and data spaces as shown in Fig. 4. This is the reason why we can apply the smoothing independently of the target shape. Please note that if the curvature of the concave area of the target shape is larger, $|d^2y_{0.5}/dx_{0.5}^2|$ becomes larger as well, which can lead to that the smoothing in the real space is the best to suppress the maximum error. However, for most cases, the fractional transform space ($\alpha = 0.5$) works well to some extent even if we do not have any information about the target shape.

6. Optimization of the Fractional Transform Parameter

6.1 Parameter Optimization

The smoothing method described in the previous section utilizes a constant parameter α . However, the accuracy of estimation using this method is not the best among the 3 methods discussed, including the conventional ones. This is because the parameter α is constant and is independent of the target shape. As described in the previous section, the absolute value of the 2nd derivative of the fractional transform quasi wavefront is expressed as in Eq. (21). We derive the parameter α that minimizes $\left| \frac{d^2 y_a}{dx_c^2} \right|$. This problem is equivalent to the maximization of the square of the denominator of Eq. (21) because the numerator of Eq. (21) is independent of α . For simplicity, we define $a = dy/dx$ and $b = yd^2y/dx^2$. Then, the evaluation function to maximize is expressed as

$$f(\alpha) = (1 + a^2\alpha)^3 \left\{ 1 + (a^2 + b)\alpha \right\}^2, \quad (23)$$

where the condition $0 \leq \alpha \leq 1$ is required.

The equation $f(\alpha) = 0$ has multiple roots at $\alpha = -1/a^2$ and $\alpha = -1/(a^2 + b)$. $\alpha_{\text{opt}} = 1$ holds for $b > 0$ because $f(\alpha)$ is a strictly increasing function for $b > 0$. In the case of $b \leq 0$, the shape of $f(\alpha)$ is shown in Fig. 12, where we need to consider the order of the multiple root point, the local maximum point, and the local minimum point.

The optimum parameter $\alpha = \alpha_{\text{opt}}$ is analytically expressed as follows.

1. If $0 < b$, $\alpha_{\text{opt}} = 1$. Otherwise, go to (2).
2. If $1 < -\frac{5a^2+2b}{5a^2(a^2+b)}$, $\alpha_{\text{opt}} = 1$. Otherwise, go to (3).
3. If $-\frac{1}{a^2+b} < 0$, $\alpha_{\text{opt}} = 1$. Otherwise, go to (4).
4. If $-\frac{5a^2+2b}{5a^2(a^2+b)} < 0$, go to (5). Otherwise, go to (7).
5. If $1 < -1/(a^2 + b)$, $\alpha_{\text{opt}} = 0$. Otherwise, go to (6).
6. If $1 > (1 + a^2)^3(1 + a^2 + b)^2$, $\alpha_{\text{opt}} = 0$. Otherwise, $\alpha_{\text{opt}} = 1$.
7. If $1 < -1/(a^2 + b)$, $\alpha_{\text{opt}} = -\frac{5a^2+2b}{5a^2(a^2+b)}$. Otherwise, go to (8).

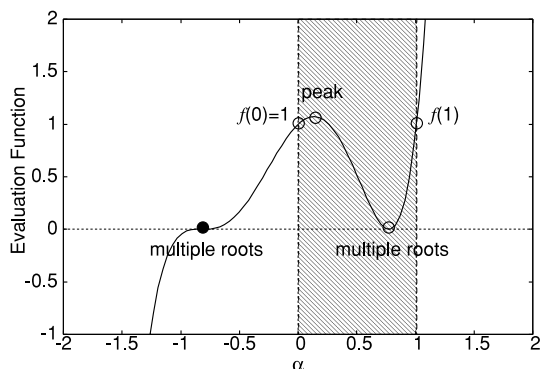


Fig. 12 The objective function $f(\alpha)$ for $b < 0$.

8. If $\frac{108b^5}{3125a^4(a^2+b)^3} > (1 + a^2)^3(1 + a^2 + b)^2$, $\alpha_{\text{opt}} = -\frac{5a^2+2b}{5a^2(a^2+b)}$. Otherwise, $\alpha_{\text{opt}} = 1$.

Note that $\frac{5a^2+2b}{5a^2(a^2+b)}$ is the α value at the local peak point, $-1/(a^2 + b)$ is the α value at the point for the double roots, $(1 + a^2)^3(1 + a^2 + b)^2 = f(1)$, and $\frac{108b^5}{3125a^4(a^2+b)^3}$ is the local peak value. Figure 13 shows the optimized parameter α_{opt} for each (a, b) . In this figure, the smoothing in the data space is optimum in the area where $\alpha_{\text{opt}} = 1$ holds. The smoothing in the real space is optimum in the area where $\alpha_{\text{opt}} = 0$ holds. On the other hand, in the area where $0 < \alpha_{\text{opt}} < 1$ holds, the smoothing in the fractional transform space is optimum. Parameters a, b are expressed by the quasi wavefront X, Y as [11]

$$a = \frac{dY/dX}{\sqrt{1 - (dY/dX)^2}}, \quad (24)$$

$$b = \frac{Yd^2Y/dX^2}{\left\{ 1 - \left(\frac{dY}{dX} \right)^2 \right\} \left\{ 1 - \left(\frac{dY}{dX} \right)^2 - Y \frac{d^2Y}{dX^2} \right\}}. \quad (25)$$

We can obtain the optimum parameter α_{opt} directly from the quasi wavefronts by utilizing these equations. This means that the proposed smoothing method does not spoil the fast imaging of the SEABED algorithm because the required procedure applies the FBST only twice to obtain stabilized images.

6.2 Adaptive Smoothing Using the Fractional BST with an Optimized Parameter

We propose the following adaptive smoothing method with an optimized parameter α_{opt} . First, we apply smoothing to the obtained quasi wavefronts. Next, we calculate a, b by using Eqs. (24) and (25) for each antenna position X . Then, we calculate the optimum parameter α_{opt} for each (a, b) with the procedure in the previous section. For simplicity, we quantize α_{opt} as 1 for $\alpha_{\text{opt}} > 0.5$, and 0 for $\alpha_{\text{opt}} \leq 0.5$. If $\alpha_{\text{opt}} > 0.5$, we apply IBST to the smoothed quasi wavefronts. If $\alpha_{\text{opt}} \leq 0.5$, we apply IBST to the quasi wavefronts,

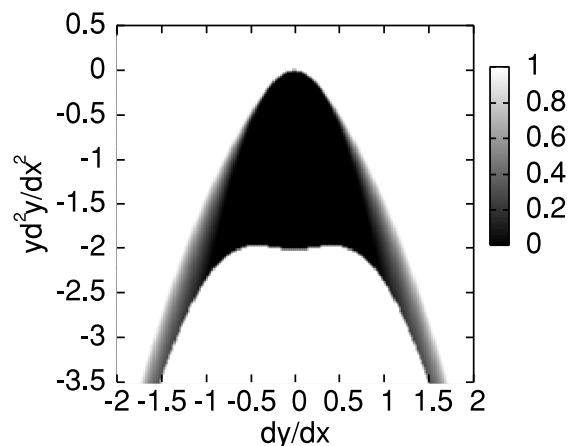


Fig. 13 The optimum fractional transform parameter.

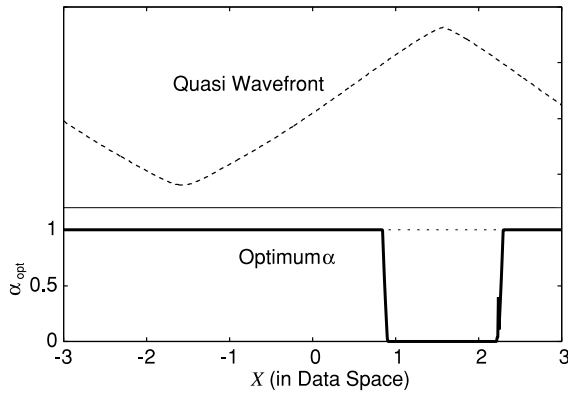


Fig. 14 The calculated optimum parameter α_{opt} .

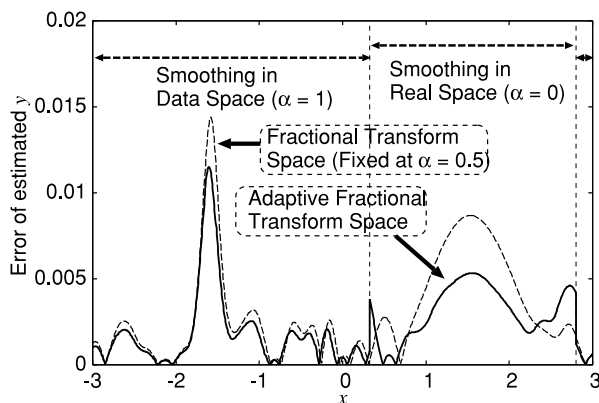


Fig. 15 Estimation error for the adaptive smoothing method.

and then we smooth the obtained image. These procedures are interpreted as smoothing in the data space ($\alpha = 1$) and smoothing in the real space ($\alpha = 0$), respectively.

We show an application example of the adaptive smoothing method explained above. We utilize preprocessing of smoothing with a correlation length of 2.5×10^{-2} of a wavelength, which is the same as the one in the section above. We empirically set the correlation length of 0.5 of a wavelength for calculations of a, b and a correlation length of 0.1 of a wavelength for smoothing in data or real spaces. The true target shape is the same one as in Fig. 6. The calculated α_{opt} is shown in Fig. 14, where the quasi wavefront is also displayed for a reference. We see the optimum parameter α_{opt} is equal to 0 or 1 for most x , because the α_{opt} in Fig. 13 has small area where $0 < \alpha_{opt} < 1$ holds. The estimation error of the adaptive smoothing method is shown as a solid line in Fig. 15. The plotted lines are the absolute values of the errors. The broken line in this figure is smoothing with a constant parameter $\alpha = 0.5$. The adaptive smoothing method adaptively selects the suitable smoothing method depending on the shape of the received data by switching $\alpha = 0$ and 1. Please note that the areas for $\alpha = 0$ and $\alpha = 1$ are different for Figs. 14 and 15 because these figures show different spaces; the data and real spaces, respectively. The areas for $\alpha = 0$ and $\alpha = 1$ changes by applying the FBST to the data. This figure shows that the smoothing method

remarkably improves the accuracy of the shape estimation. The proposed adaptive smoothing improves the maximum estimation error by 1.2 times compared to the smoothing method with a fixed parameter. This improvement corresponds to 1.6 dB in terms of the S/N.

7. Conclusion

In this paper, we proposed an image stabilization algorithm for the SEABED algorithm, a fast imaging algorithm for UWB pulse radars. First, we proposed a FBST, which was obtained by expanding a conventional BST utilized in the SEABED algorithm. By utilizing the FBST, we can deal with an intermediate space between the real and data spaces. The smoothness of data is guaranteed in the intermediate space regardless of the target shape. Therefore, smoothing in the intermediate space does not spoil imaging accuracy. The proposed smoothing method with a fixed parameter gives a 1.5 times improvement in accuracy compared to the conventional method. Next, we proposed an adaptive smoothing method by adaptively selecting the optimum parameter of the fractional transform. The optimum parameter is analytically derived, and we utilized the parameter to stabilize the estimated image. The application examples here showed that the proposed algorithm with a fixed parameter can stabilize the image regardless of the target shape. Additionally, we confirmed that the adaptive smoothing method enhances the accuracy of estimations compared to the conventional methods.

Acknowledgment

We thank Prof. Toru Sato at the Department of Communications and Computer Engineering, Graduate School of Informatics, Kyoto University, Japan for his valuable advice.

References

- [1] E.J. Bond, X. Li, S.C. Hagness, and B.D. van Veen, "Microwave imaging via space-time beamforming for early detection of breast cancer," *IEEE Trans. Antennas Propag.*, vol.51, no.8, pp.1690-1705, 2003.
- [2] R.M. Narayanan, X. Xu, and J.A. Henning, "Radar penetration imaging using ultra-wideband (UWB) random noise waveforms," *IEE Proc.-Radar Sonar Navig.*, vol.151, no.3, pp.143-148, 2004.
- [3] J. van der Kruk, C.P. A. Wapenaar, J.T. Fokkema, and P.M. van den Berg, "Three-dimensional imaging of multicomponent ground-penetrating radar data," *Geophysics*, vol.68, no.4, pp.1241-1254, 2003.
- [4] C.J. Leuschen and R.G. Plumb, "A matched-filter-based reverse-time migration algorithm for ground-penetrating radar data," *IEEE Trans. Geosci. Remote Sens.*, vol.39, no.5, pp.929-936, May 2001.
- [5] T.J. Cui, Y. Qin, G.L. Wang, and W.C. Chew, "High-order inversion formulas for low-frequency imaging of 2D buried targets," *Proc. 2004 IEEE Antennas and Propagation Society International Symposium*, vol.1, pp.189-192, 2004.
- [6] W.C. Chew and Y.M. Wang, "Reconstruction of two dimensional permittivity distribution using the distorted Born iterative method," *IEEE Trans. Med. Imaging*, vol.9, no.2, pp.218-225, 1990.
- [7] P. Lobel, C. Pichot, L. Blanc-Feraud, and M. Barlaud, "Microwave imaging: Reconstructions from experimental data using conjugate

- gradient and enhancement by edge-preserving regularization,” *International Journal of Imaging Systems and Technology*, vol.8, no.4, pp.337–342, Dec. 1998.
- [8] T. Sato, T. Wakayama, and K. Takemura, “An imaging algorithm of objects embedded in a lossy dispersive medium for subsurface radar data processing,” *IEEE Trans. Geosci. Remote Sens.*, vol.38, no.1, pp.296–303, 2000.
- [9] T. Sakamoto and T. Sato, “A target shape estimation algorithm for pulse radar systems based on boundary scattering transform,” *IEICE Trans. Commun.*, vol.E87-B, no.5, pp.1357–1365, May 2004.
- [10] T. Sakamoto and T. Sato, “Fast imaging of a target in inhomogeneous media for pulse radar systems,” *Proc. 2004 IEEE International Geoscience and Remote Sensing Symposium*, vol.3, pp.2070–2073, Sept. 2004.
- [11] T. Sakamoto and T. Sato, “A phase compensation algorithm for high-resolution pulse radar systems,” *IEICE Trans. Commun.*, vol.E87-B, no.11, pp.3314–3321, Nov. 2004.
- [12] T. Sakamoto and T. Sato, “A phase compensation algorithm for high-resolution pulse radar systems,” *Proc. 2004 International Symposium on Antennas and Propagation*, pp.585–588, Aug. 2004.
- [13] T. Sakamoto and T. Sato, “A fast algorithm of 3-dimensional imaging for pulse radar systems,” *Proc. 2004 IEEE AP-S International Symposium and USNC/URSI National Radio Science Meeting*, vol.2, pp.2099–2102, June 2004.
- [14] T. Sakamoto, S. Kidera, T. Sato, T. Mitani, and S. Sugino, “An experimental study on a fast imaging algorithm for UWB pulse radar systems,” *Proc. 2005 IEEE AP-S International Symposium and USNC/URSI National Radio Science Meeting*, P24.5, July 2005.



Takuya Sakamoto was born in Nara, Japan in 1977. Dr. Sakamoto received his B.E. degree from Kyoto University in 2000, and M.I. and Ph.D. degrees from the Graduate School of Informatics, Kyoto University in 2002 and 2005, respectively. He is a research associate in the Department of Communications and Computer Engineering, Graduate School of Informatics, Kyoto University. His current research interest is in digital signal processing. He is a member of the IEEJ and the IEEE.